Visualization of intracellular lipid droplets using lipophilic benzothiazole-based push-pull fluorophores at ultralow concentration

Mauro Safir Filho, Pascal Dao, Anthony Martin, Rachid Benhida

Visualization of intracellular lipid droplets using lipophilic benzothiazole-based push-pull fluorophores at ultralow concentration.

Mauro Safir Filho,[†,a,b] Pascal Dao,[†,a] Anthony R. Martin,*[a] and Rachid Benhida,*[a,c]

[a] Université Côte d'Azur, CNRS, Institut de Chimie de Nice UMR7272, Nice, France.

[b] CAPES Foundation, Ministry of Education of Brazil, Brasília DF 70040-020, Brazil

[c] Mohamed VI Polytechnic University, UM6P, 43150 Ben Guerir, Morocco

* corresponding authors: anmartin@unice.fr, benhida@unice.fr

Abstract

In this study we describe the development of new lipophilic and biocompatible benzothiazole-based push-pull fluorophores as potent fluorogenic probes for the specific staining of intracellular lipid droplets (LDs) at ultralow concentration (≤ 100 nM). These new fluorophores, harboring a D-π-A framework featuring an extended π-conjugated spacer, a lipophilic tertiary amine (D) and hydrophobic aryl groups (A), were prepared by an efficient and practical synthetic route. The photophysical studies of these compounds underlined their high polarity sensitivity, characterized by a strong solvatochromic effect and the large Stokes shifts values (λ_{em} 465-630 nm, $\Delta\lambda$ up to 6751 cm^{-1}). Finally, the *in cellulo* investigations of **D1** revealed its ability to selectivity accumulate in LDs and to allow their remarkable visualization using confocal fluorescence microscopy.

Keywords: benzothiazole fluorophores, push-pull fluorophores, lipid droplets, confocal microscopy

Introduction

Lipid droplets (LDs) are cytoplasmic organelles involved in the storage of neutral lipids. They are composed of a core of hydrophobic neutral lipids surrounded by a phospholipid monolayer membrane and associated proteins of the PAT protein family (Perilipin, Adipocyte differentiation-related protein (ADRP) and TIP47 proteins (tail-interacting protein of 47 kDa)).[1] The degradation of LDs provides metabolic energy for different cellular process such as membrane formation, trafficking, or protein-protein interactions. The deregulation of LDs functions can lead to metabolic or immune disorders, as well as cancer.[2] Despite the recent advances in the understanding of biological properties and functions of LDs, the development of more specific and powerful tools dedicated to the visualization of LDs may further foster our deep understanding of the role of these peculiar organelles.

In this context, fluorescence imaging techniques are one of the most powerful and popular tools for biomedical research, both for *in cellulo* and *in vivo* studies. The development of robust and fine-tuned fluorescent probes featuring high brightness, chemo/photostability and target selectivity significantly bolstered the ways to monitor and study biochemical changes of specific cellular compartments.[3] Of note, fluorescence imaging offers a versatile, biocompatible and non-invasive approach to track and

probe cellular organelles[4–6] and visualize local physicochemical changes such as the viscosity[7,8] and the pH.[9] Fluorescence imaging also enables the signaling of chemical analytes[10,11] or enzymes[12,13] with the advantages of its high sensitivity, low cost, user friendliness and possible temporal/spatial resolution.

Heretofore, only few examples of fluorescent probes for LD staining have been reported. Among them, the most popular and commercially available probes to visualize these structures include Nile Red[14] and BODIPY (493/503, 540)[15] fluorophores. However, these probes display important limitations. In fact, they need to be used as dilute solutions, as their fluorescence emission is highly suppressed at high-concentrations; possibly through an aggregation-caused quenching (ACQ). BODIPY fluorophores can selectively accumulates in LDs, but their reduced Stokes shift usually accounts for the self-deactivation of the excited fluorophore *via* non-radiative energy transfer. This non-radiative decay leads to weak fluorescence intensity and interference from the scattered excitation light that causes strong background artifacts. Conversely, the solvatochromic Nile Red dye shows poor selectivity towards LDs and usually stains other hydrophobic compartments within the cells. Moreover, it also shows broad absorption and emission spectra, hence hampering its use for multicolour imaging. To overcome such drawbacks and enhance the staining stability and selectivity for lipid droplets, the quest for new fluorogenic probes with superior photophysics and different operation modes was undertaken.[16] Prospective advances in molecular platforms for LDs staining have been recently published, exploiting numerous hydrophobic fluorogenic probes including AIEgens (aggregation induced emission luminogens),[17–22] solvatochromic StatoMerocyanine dyes,[23] and solvatofluorochromic fluorophores displaying emission from intramolecular charge transfer excited states.[24–27]

In our laboratory, we have recently developed a new set of environment responsive D-π-A fluorophores and demonstrated their high biocompatibility, fine-tuned spectroscopic properties, and their smooth chemical transformation into molecular probes for biological applications.[28,29] The molecular structures of our fluorophores encompass an electron donating 6-aminofunctionalized benzothiazole scaffold (D) which is connected *via* a single vinyl linker to different electron acceptor aryl groups (A) (Fig. 1). The straightforward and diversity-orientated synthetic pathway to access these compounds has enabled the preparation of 20 different fluorophores featuring high brightness and remarkable solvatofluorochromism.[28] Thereafter, these fluorophores were successfully employed to develop highly sensitive probes to monitor β-galactosidase activity during early stages of cellular senescence.[29]

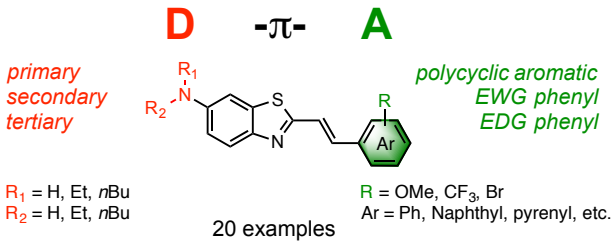

Figure 1. General structure of the benzothiazole-based styryl fluorophores previously reported by our group.[28,29]

Results and discussion

Building on our prior work on benzothiazole-based push-pull fluorophores adaptable for biomedical applications, we have developed a new set of highly lipophilic fluorogenic probes that are adapted to the intracellular staining of LDs. For this purpose, we designed a new set of fluorophores that features a lipophilic 6-*N*-ethyl-*N*'-butylaminobenzothiazole as the electron donating group (D), an extended vinyl-phenylacetylene spacer as a π-conjugated linker and a hydrophobic terminal aryl (A) motif (Fig. 2). Herein, we disclose the photophysical characterization of these novel structures by UV-Vis absorption and steady-state fluorescence emission spectroscopies and exemplify their use for intracellular lipid droplet visualization by confocal microscopy.

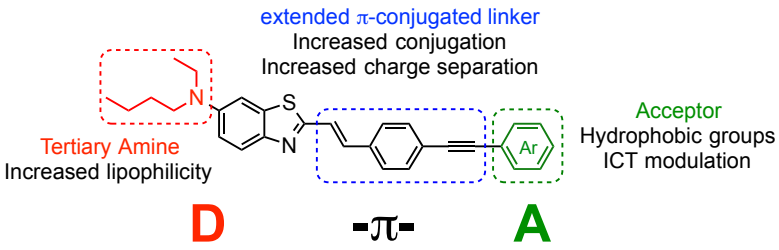

Figure 2. General structure of the benzothiazole-based push-pull fluorophores explored in this work.

The scaffold design presented in Fig.2 should grant access to fluorophores exhibiting high lipophilicity and improved photophysical properties in terms of absorption maxima, brightness and Stokes shift. Thus, a plain phenyl ring, analogs harboring electron withdrawing groups (4-methylbenzoate and 4-formylphenyl) and polycyclic aromatic hydrocarbons (9-phenanthryl, 4-biphenyl and 1-naphthyl) were selected as acceptor moieties (A) in order to build up a large charge transfer character of the dyes in the excited state (Table 1). In parallel, we also expected that the use of an extended π-conjugated spacer could be beneficial for: (i) the redshift of the absorption maxima; (ii) increased charge separation between the donor and the acceptor groups in the excited state, which may also enhance the dye sensitivity to solvent polarity; and (iii) a contribution to enhance the lipophilicity of the dyes. Finally, we selected a lipophilic tertiary *N*-ethyl-*N*-butylamino function as the donor group (D).

Table 1. Chemical structure of the benzothiazole-based push-pull fluorophores studied in this work.

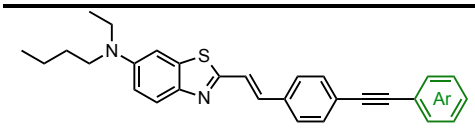

Dye	Aryl
D1	Phenyl
D2	1-naphthyl
D3	9-phenanthryl
D4	4-biphenyl
D5	4-formylphenyl
D6	4-methylbenzoate

Synthesis

The first step of our study consisted of the synthesis of the bromo-containing dye precursor **2** and its subsequent decoration with different arylacetylene groups *via* Sonogashira cross coupling reactions using selected arylacetylenes. Dye precursor **2** was synthesized in a one-pot two-step synthetic route (Scheme 1) involving a Knoevenagel condensation between the *p*-bromobenzaldehyde and the 6-*N*-ethylaminobenzothiazole derivative (**1**), followed by the direct alkylation of the *N*-ethylamino group using 1-iodobutane. Thus, benzothiazole derivative **1** was engaged in a Knoevenagel condensation using a slight excess of *p*-bromobenzaldehyde (1.3 equiv.) and a stoichiometric amount of potassium hydroxide, in *N,N*-dimethylformamide at room temperature. Then, alkylation of this intermediate using *n*-iodobutane, in the presence of potassium carbonate, smoothly afforded the dye precursor **2** in a satisfactory 52% yield. With precursor **2** in hand, we proceeded with its connection to various arylacetylene scaffolds *via* a Sonogashira cross-coupling reaction. This reaction was performed under palladium catalysis, using $[Pd(PPh_3)_4]$ and copper iodide in the presence of 1.5 equivalents of the corresponding arylacetylene. The target fluorophores **D1-D6,** whose structures are summarized on Scheme 1, were obtained in moderate to good yields (23-67 %) after purification by preparative thin layer chromatography.

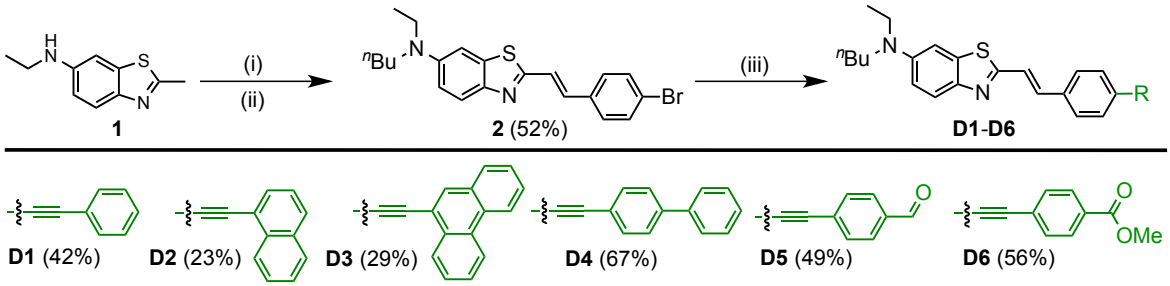

Scheme 1. Synthetic preparation of dye **D1-D6**. *Reagents and conditions* (i) *p*-bromobenzaldehyde (1.3 equiv.), KOH (1.0 equiv.), DMF, r.t., overnight; (ii) 1-iodobutane (3.0 equiv.), K_2CO_3 (1.0 equiv.), DMF, 80°C, overnight. (iii) arylacetylene (1.5 equiv.), $[Pd(PPh_3)_4]$ (20 mol%), CuI (15 mol%), DMF:TEA (1:1), 50°C, 12 h.

Spectroscopic Studies

UV-Visible Absorption

Once these new compounds (**D1-D6**) were characterized by ^1H and ^{13}C NMR spectroscopies and high-resolution mass spectrometry, we investigated on their photophysical properties in different solvents: cyclohexane (Cyhex), 1,4-dioxane, ethyl acetate (EA), acetonitrile (MeCN), dimethyl sulfoxide (DMSO) and methanol (MeOH). Figure 3 and 4 depict the UV-Vis absorption and fluorescence emission spectra for these six fluorophores in three of the aforementioned solvents.[30] Table 1 summarizes the main photophysical data.

As a general trend, all these fluorophores present two intense absorption bands localized in the near ultraviolet (~ 318 - 356 nm, λ_{abs1}) and visible (~ 419 - 446 nm, λ_{abs2}) spectral regions. These bands should be associated with the excitation of these fluorophores to an upper electronic excited state ($S_1 \rightarrow S_n$ transition) and to the lowest energetic S_1 state ($S_0 \rightarrow S_1$ transition), respectively. In addition, high molar extinction coefficient values were recorded regardless of the maxima (λ_{abs1} or λ_{abs2}) that was considered (ε =

24.6 - 39.7 × 10^4 $M^{-1}.cm^{-1}$, λ_{abs1}; 35.0 - 53.3 x 10^4 $M^{-1}.cm^{-1}$, λ_{abs2}); they are in agreement with a π–π* transitions. Interestingly, both absorption bands exhibited very weak charge transfer character which is accounted for the moderate solvatochromic effect that was observed for all the dyes. In fact, when changing from the least to the most polar solvent the absorption maxima are red-shifted by only 8-17 nm. Regarding the absorption spectra, the maxima in the near-UV region (λ_{abs1}) are shifted to longer wavelength for the molecules harboring the larger frameworks (1-naphthyl and 9-phenanthryl, dyes **D2** and **D3**, respectively) compared with the dyes **D1, D4-D6**. Conversely to λ_{abs1}, all the dyes displayed λ_{abs2} values in a narrow range (Table 1). Moreover, compared with our previous work where the donor and the acceptor were separated by a single vinyl π-spacer, the lowest energy electronic transitions are significantly red-shifted (~ 30 nm).[28] This is a clear consequence of the larger π-spacer that is used in the present study.

Table 2. Main photophysical data of the fluorophores **D1**-**D6**.

Dye	Solvent	ε^a	λ_{abs1}/ $\lambda_{abs2}{}^b$	$\lambda_{em}{}^b$	$\Delta\lambda^c$	$\Phi_{fl}{}^d$
D1	Cyclohexane	27.5/42.2	318/419	465/495	3664	0.53
	1,4-Dioxane	28.0/40.4	321/424	516	4205	0.76
	Ethyl acetate	27.4/38.8	322/421	539	5200	0.64
	DMSO	24.6/35.0	326/436	593	6072	0.93
	MeCN	28.2/38.9	322/426	578	6173	0.63
	MeOH	26.2/35.8	322/429	563	5548	0.58
D2	Cyclohexane	25.5/47.3	342/422	468/500	3696	0.60
	1,4-Dioxane	27.1/46.3	349/427	518	4114	0.71
	Ethyl acetate	26.8/44.4	344/424	545	5236	0.70
	DMSO	25.6/40.0	356/439	603	6195	0.94
	MeCN	28.7/44.7	345/426	584	6350	0.76
	MeOH	28.0/41.2	350/429	567	5673	0.54
D3	Cyclohexane	23.8/40.4	346/424	470/503	3704	0.86
	1,4-Dioxane	24.4/39.0	348/427	523	4298	0.92
	Ethyl acetate	25.5/40.1	350/425	548	5281	0.56
	DMSO	25.9/36.1	355/440	609	6306	0.88
	MeCN	27.4/39.0	350/430	590	6306	0.79
	MeOH	27.2/38.9	352/432	573	5696	0.65
D4	Cyclohexane	36.2/53.3	327/421	467/498	3672	0.75
	1,4-Dioxane	37.8/52.2	331/426	516	4094	0.75
	Ethyl acetate	39.4/49.8	327/423	541	5156	0.73
	DMSO	35.4/43.4	337/438	601	6262	0.99
	MeCN	39.7/47.9	329/426	581	6192	0.74
	MeOH	36.5/44.6	330/428	569	5789	0.78
D5	Cyclohexane	32.0/46.9	327/431	479/513	3708	0.65
	1,4-Dioxane	33.0/44.4	331/434	534	4314	0.87
	Ethyl acetate	37.2/47.6	330/429	574	5888	0.63
	DMSO	33.8/41.2	338/446	611	6054	<0.001
	MeCN	39.7/47.2	330/432	590	6198	<0.001
	MeOH	32.1/38.2	332/433	563	5332	0.14
D6	Cyclohexane	32.5/49.7	326/426	474/505	3672	0.82
	1,4-Dioxane	33.9/46.6	328/430	525	4208	0.95
	Ethyl acetate	35.1/46.8	327/427	558	5498	0.80
	DMSO	33.9/42.2	332/442	630	6751	0.31
	MeCN	39.5/46.9	328/431	604	6645	0.37
	MeOH	37.3/44.1	328/432	583	5995	0.26

[a] ε : molar extinction coefficient (× 10^{-3} in $(M.cm)^{-1}$); [b] λ_{abs} and λ_{em} : absorption and emission maxima (in nm), respectively; [c] $\Delta\lambda$: Stokes shift (in cm^{-1}); [d] Φ_{fl} : fluorescence quantum yield.

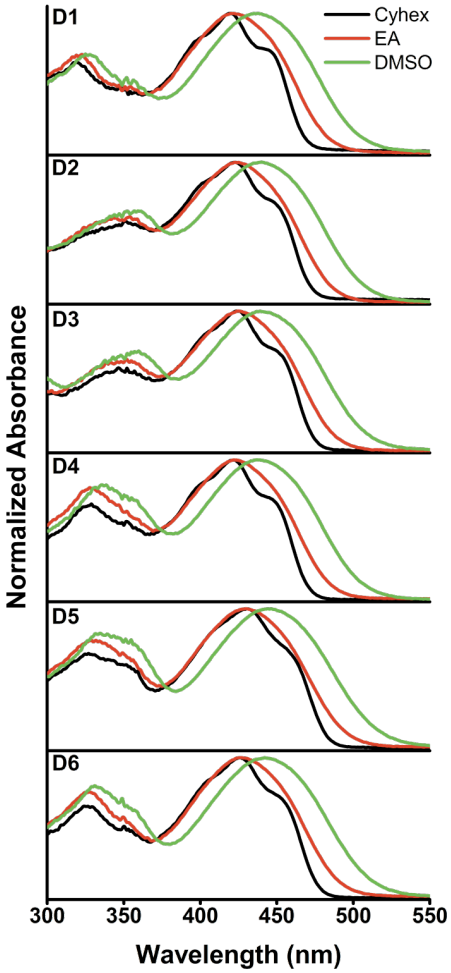

Figure 3. UV-Vis absorption spectra in different solvents of dyes **D1**-**D6**. Condition: dye concentration ≈ 10 μM; cell path length, 1 cm.

Fluorescence emission

The fluorescence emission spectra for each dye were recorded using the relevant absorption maxima (λ_{abs1} and λ_{abs2}) as the excitation wavelengths. In contrast to the ground state properties, all these six fluorophores showed remarkable red-shift in their emission maxima when going from the least polar aprotic solvent to the most polar environment (Table 2 and Fig. 4). This positive solvatofluorochromism strongly emphasizes a large charge transfer character of the S_1 excited state of dyes **D1**-**D6**. Among all fluorophores, compound **D6**, bearing the strong acceptor group 4-methylbenzoate, presented the highest degree of solvent sensitivity, with Stokes shift ($\Delta\lambda$, λ_{abs2} - λ_{em}) values up to 6751 cm^{-1} in DMSO. Analogously, no noticeable differences in the emission spectra were observed for the fluorophores featuring unsubstituted acceptor (A) groups (**D1**-**D4**). Additionally, whatever the excitation wavelength (λ_{abs1} or λ_{abs2}) the same emission spectra were recorded, which may indicate that the rate of internal conversion from upper excited states (S_n) to S_1 is very fast and fluorescence emission only takes place from the relaxed S_1 excited state (Supporting Information, Fig. S2). High fluorescence quantum yield values were observed for all dyes, except for the molecules

bearing π-electron acceptor groups (-CHO and -COOMe, **D5** and **D6**, respectively) where a decrease in the emission intensity was observed in solvents with increased polarity. It is well known that the reduced energy gap between the excited and ground states in polar solvents may favor internal conversion from the S_1 to the S_0 state and create a non-radiative tunnel to release energy. However, the particular behavior observed for dye **D5**, harboring the strong electron withdrawing formyl group, actually supports the hypothesis that the fully charge separated and non-emissive twisted intramolecular charge transfer state (TICT) may be formed. Essentially, changes in the molecular geometry associated with an internal rotation within the fluorophore can usually provide an increase in the rate of the non-radiative decay, hence causing the fluorescence quenching. Many examples of solvatochromic fluorophores displaying either weak fluorescence emission or a significant drop of the Φ_{fl} values in highly polar solvents have been associated with the formation of a putative TICT excited state.[31,32] Of note, an anomalous emission in methanol (blue shifted compared with the less polar ethyl acetate) was observed for dye **D5**. This may evidence conversion of the formyl group into an (hemi)acetal moiety, thus reducing its acceptor character.

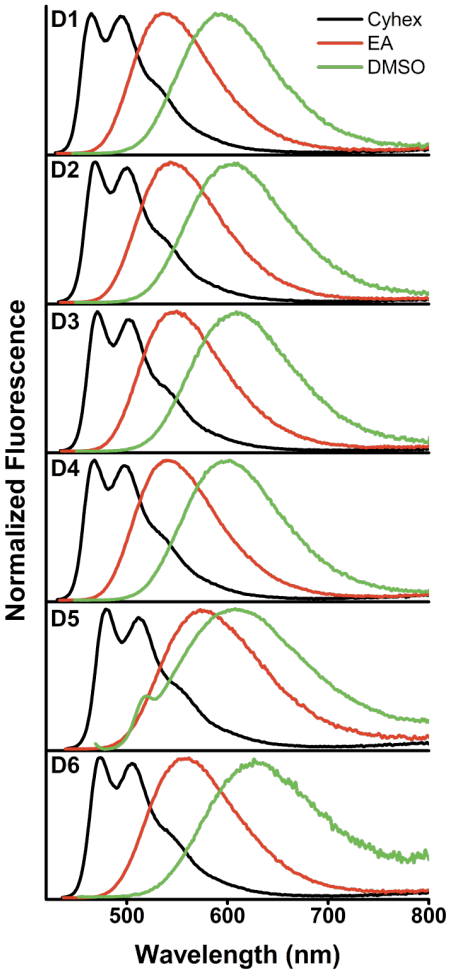

Figure 4. Fluorescence emission spectra in different solvents of dyes **D1**-**D6**. Condition: dye concentration ≈ 1 μM; cell path length, 1 cm.

Finally, the positive solvatochromism was further investigated using the Lippert-Mataga model (Fig. 5). The Stokes shift was plotted as a function of the orientation polarizability (Δf) in aprotic solvents. In all cases, linear relationships were obtained. These results support the hypothesis of an increase in the dipole moment of the excited states.

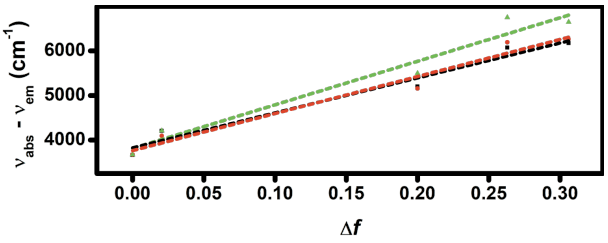

Figure 5. Dependence of the Stokes shift ($\lambda_{abs2} - \lambda_{em}$) on the Lippert-Mataga orientation polarizability paremeter for dyes **D1** (black), **D4** (red) and **D6** (green). Correlation factors R^2 are, respectively, 0.97, 0.97 and 0.96.

***In Cellulo* Imaging**

Following the investigation of the photophysical properties of these fluorophores, we assessed their applicability in the tracking of intracellular lipid droplets. For this purpose, dye **D1**, that bears a plain phenyl ring as the acceptor moiety, was selected as a simple example from the series **D1-D6** (*vide infra*). As a preliminary study, cellular imaging experiments by confocal laser scanning microscopy were performed to investigate the *in cellulo* application of **D1** in fixed cells. Since altered LD expression can marker of cancer aggressiveness,[27] we employed, in this experiment, A375 melanoma cells as a cancer cell model. After incubation of **D1** (100 nM) in A375 melanoma cancer cells for 30 minutes, an intense and selective fluorescence emission was recorded. Thus, the cellular uptake of **D1** could be confirmed (Fig. 6). The visualization under the microscope underlines that **D1** selectively accumulates in cytoplasmic dots/vesicles which are consistent in size and shape with spherical organelles such as LDs.

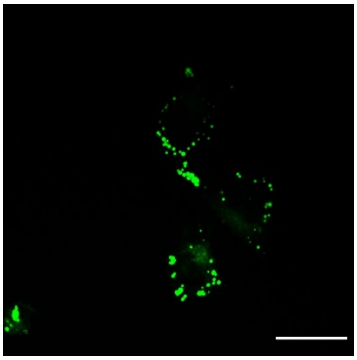

Figure 6. Cellular uptake of dye **D1**: Melanoma cells A375 were incubated with 100 nM of probes **D1** for 30 min. Scale bar 50 µM.

Following this initial experiment, we performed colocalization studies to evidence whether or not **D1** was located in LDs. Therefore, we employed the Nile Red fluorophore as the reference marker for LDs.[14] Interestingly, control experiments with specific markers of different round-shaped structures such as eea1 (endosomes) and lamp1 (lysosomes) were performed as well to definitely identify the exact location of **D1**. Satisfactorily, the results clearly underpin the selective colocalization of **D1** and Nile Red and no overlap with the two other organelles was recorded (Fig. 7). In fact, this confocal microscopy observation emphasized the higher capacity of probe **D1** for staining LDs with improved selectivity, reduced background emission and in a lower concentration than the Nile Red marker. Heretofore, few probes for the tracking of lipid droplets at ultralow concentration (≤ 100 nM) have been reported in

the literature.[17] In addition, this report is, to date, the lowest reported concentration to stain LDs in cells using solvatofluorochromic fluorophores.[24–27]

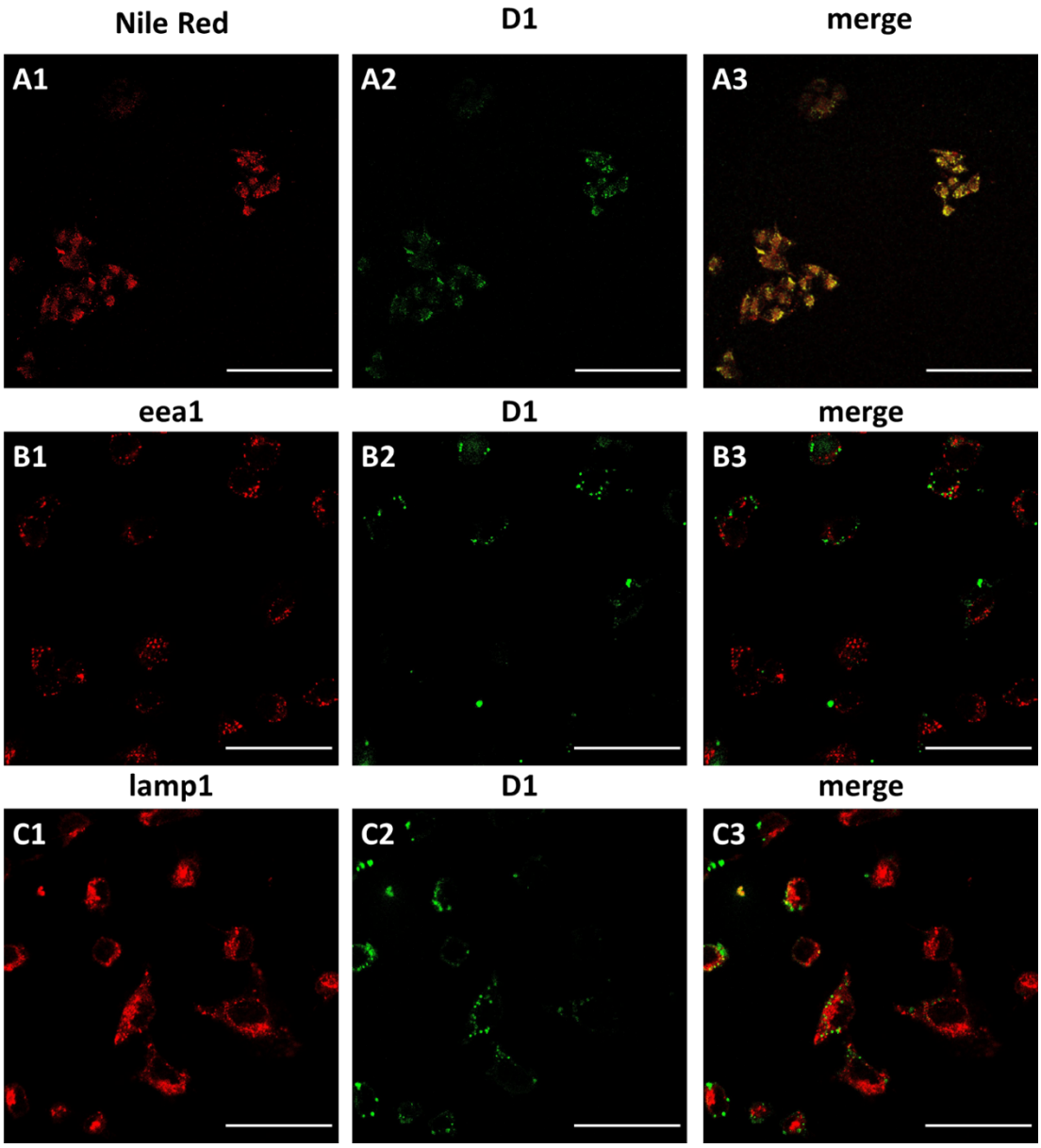

Figure 7. Confocal microscopy of melanoma cells co-stained with probe **D1** and (A) Nile Red (Lipid droplets), (B) lamp1 (lysosome) and (C) eea1 (endosome). Scale bar: 50 µm. For image A1, B1 and C1 emission was collected at 600-700 nm (λ_{ex} = 594 nm). For image A2, B2 and C2 emission was collected at 450-550 nm (λ_{ex} = 458 nm). The merged images (A3, B3 and C3) correspond to the combined green and red channels.

The excellent ability for staining LDs at submicromolar concentrations using probe **D1** may result from the synergic contribution of different factors. Notably, **D1** has an inherent and significant lipophilic character, evidenced by its high ClogP value of 10.1.[33] This value is significantly above the lower threshold value (ClogP = 5) usually required for lipid droplet staining, as estimated by Horobin and co-workers.[34] In addition, dye **D1** shows significant sensitivity to water. Indeed, while bright fluorescence emission is recorded in non-aqueous environments (*e.g.* lipid droplets, organic solvent), this emission intensity is substantially suppressed when the water content increases (*e.g.* cytosol) (Fig. 8). Thus, the combination of the highly lipophilic character of **D1** and its fluorescence quenching in aqueous environment may account for the selective staining of LDs with very low background noise.

To demonstrate the enhanced fluorescence emission of **D1** in LDs, we analysed the changes in emission in PBS solution (pH = 7.4), in the presence of incremental amounts of dispersed oleic acid droplets (0-300 μM, Fig. 9). In this case, a spectacular increase in the fluorescence intensity (> 40-fold), together with the expected blue shift in the emission maxima, was observed upon accumulation of the probe **D1** inside the lipidic vesicles. Hence, these observations strongly support the fact that **D1** displays a high affinity for LDs and its sequestration in LDs greatly enhances its fluorescence emission.

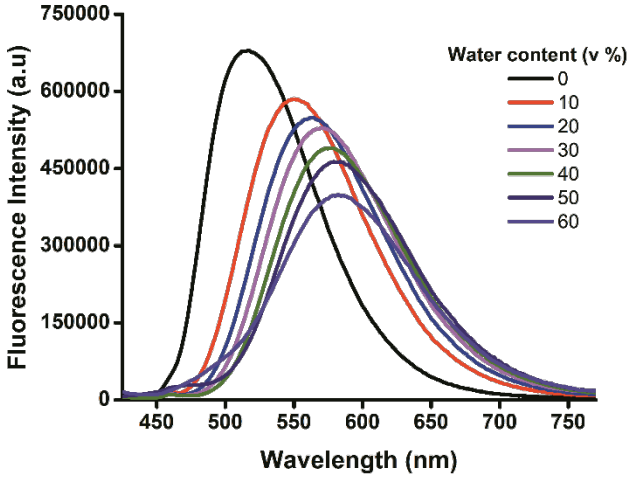

Figure 8. Fluorescence emission spectra of **D1** in response to incremental amount of H_2O in 1,4-dioxane (0-60%, v:v). Conditions: dye concentration ≈ 0.1 μM; λ_{exc} = 405 nm. (Higher water content led to the precipitation of the fluorophore).

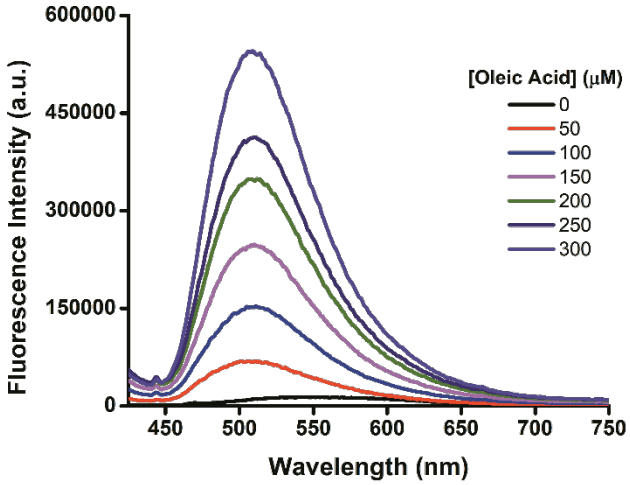

Figure 9. Fluorescence emission spectra of **D1** in PBS (pH 7.4) in the absence and after supplementation with increased amounts of oleic acid (0-300 mM). Conditions: dye concentration ≈ 0.1 μM; λ_{exc} = 405 nm.

Next, we explored the application of **D1** to monitor the accumulation of lipid droplets in cells. Fatty acids and phospholipids are essential sources of energy for the cellular machinery. Recent studies demonstrated that high levels of intracellular LDs can be closely associated with the rapid growth of cancer cells. These observations highlight that the monitoring of altered LD expression can be used as a marker of cancer aggressiveness.[27] Therefore, in this experiment, A375 melanoma cells were incubated with oleic acid (50 μM) for 24 h prior to their staining using **D1**. Of note, it is known that fatty acid supplementation of cultured cells stimulates the fatty acid receptor FFAR4, which in turn triggers the increase of LD vesicles in size and number.[35] As expected, this overproduction of lipid storage vesicles could be clearly visualized, and it was closely correlated with an increase in the fluorescence intensity compared with cells that were not supplemented with oleic acid (Fig. 10 *vs* Fig. 7A). Altogether, these results

clearly underpin that **D1** can be used as a selective and specific intracellular lipid droplet staining probe in fixed cells. It can be used either for colocalization studies or to report altered lipid metabolism associated with an extended expression of lipid storage structures. It is noteworthy that the use of **D1** at submicromolar concentration (100 nM) accounts for its superior performance compared with the Nile Red fluorophore.

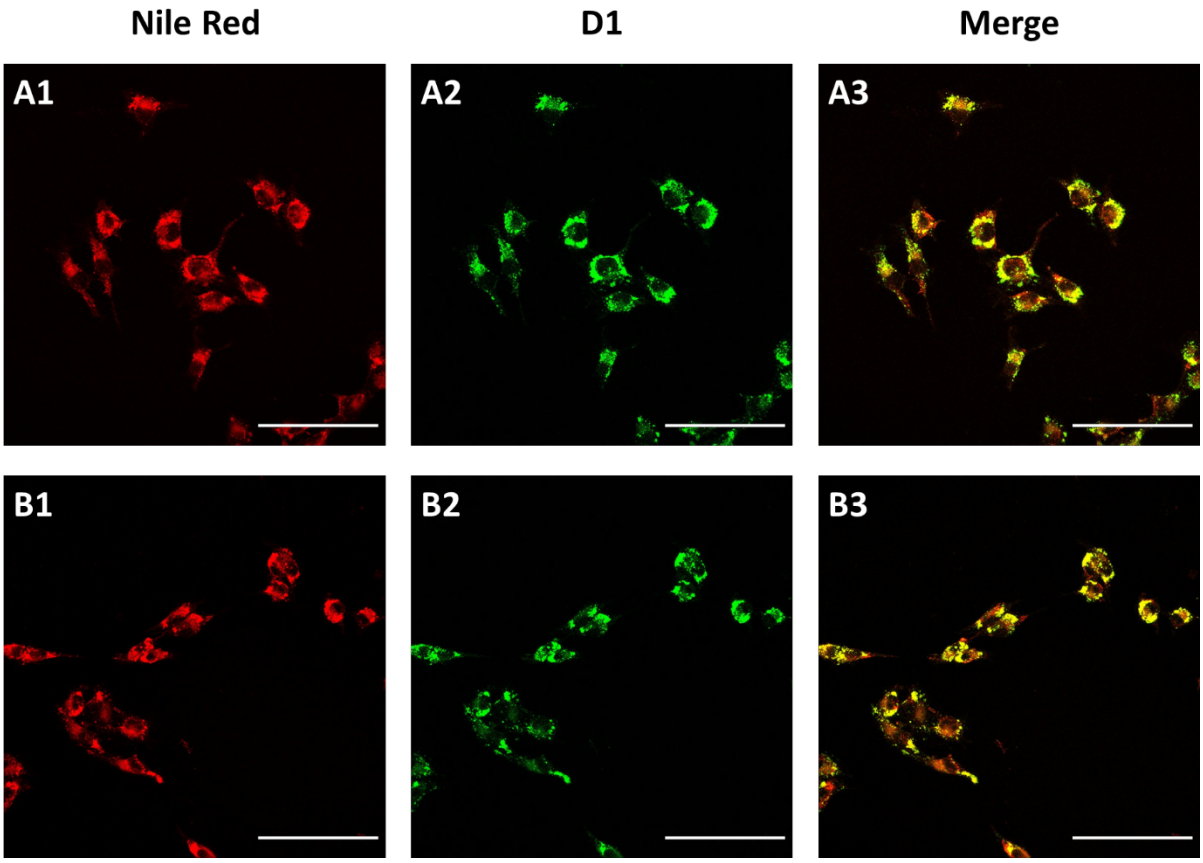

Figure 10. Confocal microscopy of melanoma cells (2 fields) exposed to oleic acid for 24 h and co-stained with probe **D1** (100 nM) and Nile Red (300 nM), as the reference marker for LDs. Scale bar: 50 µm. For image A1 and B1 emission was collected at 600-700 nm (λ_{ex} = 594 nm). For image A2 and B2 emission was collected at 450-550 nm (λ_{ex} = 458 nm). The merged images (A3 and B3) correspond to the combined green and red channels.

Conclusion

In this work a new family of highly lipophilic solvatofluorochromic fluorophores (**D1**-**D6**), exploiting a 6-aminofunctionalized benzothiazole core, were successfully designed and synthesized in a 6 steps synthetic route. The photophysical properties of **D1-D6** were studied using solutions in different solvents, using UV-visible absorption and steady-state fluorescence emission spectroscopy. These new fluorophores display very bright fluorescence emissions in all solvents. They feature two intense absorption bands, large Stokes shifts and substantial polarity sensitivity underlined by the strong positive solvatochromic effect. The fluorescence quenching in aqueous environments and the high affinity of these compounds to target hydrophobic/lipidic compartments was demonstrated. The latter could be clearly rationalized considering the high ClogP value for dye **D1**. Finally, the biocompatibility for *in cellulo* applications was also ascertained, for **D1**, and exemplified in fixed A375 melanoma cells. This study revealed the high specificity

of this dye for intracellular lipid droplets staining at ultralow probe concentration and with low background emission. Moreover, **D1** can be used to visualize changes on LD size and concentration. Following this first study concerning this family of fluorophores, we now envision the use of these as biological tools for LD tracking in applied biomedical research.

Experimental section

All solvents for absorption and fluorescence experiments were of spectroscopic grade. Absorption spectra were recorded on a Cary 4 spectrophotometer (Varian) using quartz cells of 1 cm path length. Fluorescence spectra were recorded on FluoroMax 4.0 spectrofluorometer (Jobin Yvon, Horiba). The wavelengths corresponding to the absorption maxima were used as the excitation wavelengths. Stock solutions of the solvatofluorochromic dyes were prepared in 1,4-dioxane. The samples used for spectroscopic measurements contained ≈ 1% v/v of the stock solvent. UV-vis absorption spectra were recorded using a dye concentration of *ca.* 10^{-5} M. Fluorescence emission spectra were recorded using a dye concentration of *ca.* 10^{-6} M. For the fluorescence quantum yield calculation, the refraction indexes of solvents were taken into account. Quinine sulfate in an aqueous 0.1 M $HClO_4$ solution (Φ_{fl} = 0.59) or fluorescein in 0.1 M NaOH aq. solution (Φ_{fl} = 0.89) ware used as the references.[36]. All chemical reagents were obtained from commercial sources (Aldrich, Acros, Alfa Aesar) and were used without purification. Column chromatography was performed with flash silica gel (40–63 mm). Preparative TLC was performed using 20 × 20 cm, 500 μM silica gel plates (Analtech). All NMR spectra (^{1}H, ^{13}C) were recorded on a Bruker Advance Spectrometer 400. ^{1}H NMR (400 MHz) and $^{13}C\{^{1}H\}$ NMR (101 MHz) spectra were obtained with samples dissolved in $CDCl_3$ or CD_2Cl_2, with the solvent or residual solvent signals as internal references: 7.26 ppm for $CHCl_3$ and 5.32 ppm for CD_2Cl_2 for ^{1}H NMR experiments, and 77.16 ppm for $CDCl_3$ and 53.84 ppm for CD_2Cl_2 for ^{13}C NMR experiments.[37] Chemical shifts (δ) are given in ppm to the nearest 0.01 (^{1}H) or 0.1 ppm (^{13}C). The coupling constants (*J*) are given in Hertz (Hz). The signals are reported as follows: chemical shift, multiplicity (s = singlet, d = doublet, t = triplet, m = multiplet, dd = doublet of doublets), coupling constants (*J*) and integration. High Resolution Mass Spectra (HRMS) were recorded on a ThermoFisher Q Exactive (ESIMS) at a resolution of 140000 at m/z 200. Supplementary data associated with this article include: photophysical characterizations, copies of NMR spectra - see Supporting Information for more details.

Synthetic Procedures

Synthesis of dye 2

Precursor **1** (1.0 equiv.) in DMF (0.2 M), potassium hydroxide (1.0 equiv.) and corresponding aldehyde (1.3 equiv.) were stirred overnight at room temperature. After complete conversion of the starting material (TLC monitoring), the base was filtered off and 3 equivalents of 1-iodobutane and a stoichiometric amount of potassium carbonate were added. The mixture was heated at 80°C overnight. The solvent was removed in *vacuo*, and the crude material was purified by flash column chromatography on silica gel using a cyclohexane/ethyl acetate mixture as the eluent (9/1, v/v). Finally, recrystallization from methanol afforded the desired dyes

in good yield and satisfactory purity for the following steps. Yield 52 %. ^{1}H NMR (400 MHz, $CDCl_3$) δ 7.78 (d, *J* = 9.1 Hz, 1H), 7.51 (d, *J* = 8.5 Hz, 2H), 7.40 (d, *J* = 8.5 Hz, 2H), 7.34 (d, *J* = 16.2 Hz, 1H), 7.25 (t, *J* = 16.2 Hz, 1H), 6.98 (d, *J* = 2.4 Hz, 1H), 6.86 (dd, *J* = 9.1, 2.5 Hz, 1H), 3.43 (q, *J* = 7.1 Hz, 2H), 3.35 (t, *J* = 7.5 Hz, 2H), 1.66 – 1.62 (m, 2H), 1.42 – 1.34 (m, 2H), 1.20 (t, *J* = 7.0 Hz, 3H), 0.98 (t, *J* = 7.3 Hz, 3H).^{13}C NMR (101 MHz, $CDCl_3$) δ 161.0, 146.8, 145.1, 137.2, 135.1, 133.6, 132.2, 128.6, 123.5, 123.5, 122.8, 112.9, 101.8, 50.8, 45.6, 29.8, 20.5, 14.2, 12.5. HRMS (ESI) m/z: $[M+H]^+$ Calcd for $C_{21}H_{24}BrN_2S$ 415.0844; Found 415.0840.

Synthesis of dyes D1-D6

Bromide derivative **2** (0.1 mmol, 1.0 equiv.), $[Pd(PPh_3)_4]$ (20 mol%), CuI (10 mol%) and the corresponding aryl alkyne (1.5 equiv) were suspended in DMF/TEA (1:1, 0.05 M) and heated at 50°C overnight. The mixture was diluted with ethyl acetate (5 mL), filtered through a bed of celite and washed with a solution of EDTA disodium salt (0.1 M, 3 × 5 mL). The organic phase was dried over $MgSO_4$ and concentrated in *vacuo*. The crude material was purified by preparative thin layer chromatography using a mixture of cyclohexane and ethyl acetate as the eluent. Dyes **D1-D6** were obtained as bright solids.

Dye **D1.** The crude product was purified using cyclohexane/ethyl acetate (9/1, v/v) as the eluent. Yield 42 %. ^{1}H NMR (400 MHz, CD_2Cl_2) δ 7.74 (d, *J* = 9.1 Hz, 1H), 7.56 – 7.54 (m, 6H), 7.41 – 7.37 (m, 4H), 7.32 (d, *J* = 16.2 Hz, 1H), 7.02 (d, *J* = 2.5 Hz, 1H), 6.87 (dd, *J* = 9.1, 2.5 Hz, 1H), 3.44 (q, *J* = 7.0 Hz, 2H), 3.34 (t, *J* = 7.8 Hz, 2H), 1.67 – 1.61 (m, 2H), 1.45 – 1.35 (m, 2H), 1.20 (t, *J* = 7.0 Hz, 3H), 0.98 (t, *J* = 7.4 Hz, 3H). ^{13}C NMR (101 MHz, CD_2Cl_2) δ 161.1, 147.2, 145.4, 137.6, 136.4, 134.1, 132.4, 131.9, 128.8, 127.4, 124.0, 123.7, 123.6, 123.5, 113.1, 102.1, 91.2, 89.7, 51.0, 45.8, 30.0, 20.7, 14.2, 12.5. HRMS (ESI) m/z: [M + H]+ Calcd for $C_{29}H_{29}N_2S$ 437.2051; Found 437.2046.

Dye **D2.** The crude product was purified using cyclohexane/ethyl acetate (9/1, v/v) as the eluent. Yield 23 %. ^{1}H NMR (400 MHz, $CDCl_3$) δ 8.45 (d, *J* = 8.3 Hz, 1H), 7.87 (t, *J* = 8.3 Hz, 2H), 7.79 (t, *J* = 8.2 Hz, 2H), 7.67 – 7.60 (m, 3H), 7.58 – 7.53 (m, 3H), 7.47 (dd, *J* = 8.1, 7.3 Hz, 1H), 7.41 (d, *J* = 16.2 Hz, 1H), 7.32 (d, *J* = 16.2 Hz, 1H), 6.99 (d, *J* = 2.5 Hz, 1H), 6.87 (dd, *J* = 9.1, 2.5 Hz, 1H), 3.44 (q, *J* = 7.1 Hz, 2H), 3.33 (t, *J* = 7.8 Hz, 2H), 1.67 – 1.59 (m, 2H), 1.43 – 7.35(m, 2H), 1.21 (t, *J* = 7.0 Hz, 3H), 0.99 (t, *J* = 7.3 Hz, 3H).^{13}C NMR (101 MHz, $CDCl_3$) δ 161.2, 146.8, 145.1, 137.3, 136.1, 134.2, 133.4, 132.2, 130.6, 129.0, 128.5, 127.1, 126.9, 126.6, 126.3, 125.4, 123.7, 123.6, 123.5, 120.9, 112.9, 101.8, 94.5, 89.3, 50.8, 45.6, 29.8, 20.5, 14.2, 12.5. HRMS (ESI) m/z: [M + H]+ Calcd for $C_{33}H_{31}N_2S$ 487.2208; Found 487.2205.

Dye **D3.** The crude product was purified using cyclohexane/ethyl acetate (9/1, v/v) as the eluent. Yield 29 %. ^{1}H NMR (400 MHz, CD_2Cl_2) δ 8.74 – 8.70 (m, 1H), 8.69 (d, *J* = 8.2 Hz, 1H), 8.57 – 8.54 (m, 1H), 8.11 (s, 1H), 7.91 (d, *J* = 7.4 Hz, 1H), 7.76 – 7.67 (m, 6H), 7.65 – 7.60 (m, 3H), 7.41 (d, *J* = 16 Hz, 1H), 7.34 (d, *J* = 16.2 Hz, 1H), 7.02 (d, *J* = 2.4 Hz, 1H), 6.86 (dd, *J* = 9.1, 2.5 Hz, 1H), 3.43 (q, *J* = 7.0 Hz, 2H), 3.33 (t, *J* = 7.8 Hz, 2H), 1.66 – 1.62 (m, 2H), 1.42 – 1.34 (m, 2H), 1.19 (t, *J* = 7.0 Hz, 3H), 0.98 (t, *J* = 7.3 Hz, 3H).^{13}C NMR (101 MHz, CD_2Cl_2) δ 161.1, 147.2, 145.4, 137.6, 136.6, 134.1, 132.5, 132.3, 131.6, 131.4, 130.7, 130.5, 129.0, 128.1, 127.6, 127.6, 127.5, 127.4, 127.2, 124.1, 123.7, 123.6, 123.3, 123.0, 119.8, 113.1, 102.1, 94.4, 89.5, 51.0, 45.8, 30.1, 30.0, 20.8, 14.2, 12.5. HRMS (ESI) m/z: [M + H]+ Calcd for $C_{37}H_{33}N_2S$ 537.2364; Found 537.2362.

Dye **D4.** The crude product was purified using cyclohexane/ethyl acetate (9/1, v/v) as the eluent. Yield 67 %. ^{1}H NMR (400 MHz, CD_2Cl_2) δ 7.74 (d, *J* = 9.1 Hz, 1H), 7.65 – 7.58 (m, 6H), 7.58 (m, 4H), 7.47 (t, *J* = 7.6 Hz, 2H), 7.49 – 7.36 (m, 2H), 7.32 (d, *J* = 16.2 Hz, 1H), 7.02 (d, *J* = 2.5 Hz, 1H), 6.87 (dd, *J* = 9.1, 2.5 Hz, 1H), 3.44 (q, *J* = 7.0 Hz, 2H), 3.34 (t, *J* = 7.8 Hz, 1H), 1.67 – 1.59 (m, 2H), 1.45 – 1.37 (m, 2H), 1.20 (t, *J* = 7.0 Hz, 3H), 0.98 (t, *J* = 7.4 Hz, 3H). ^{13}C NMR (101 MHz, CD_2Cl_2) δ 161.1, 147.2, 145.4, 141.5, 140.6, 137.6, 136.4, 134.1, 132.4, 132.3, 129.3, 128.1, 127.5, 127.4, 127.3, 124.0, 123.7, 123.6, 122.4, 113.1, 102.1, 91.2, 90.4, 51.0, 45.8, 30.0, 20.8, 14.2, 12.5. HRMS (ESI) m/z: [M + H]+ Calcd for $C_{35}H_{33}N_2S$ 513.2364; Found 513.2359.

Dye **D5.** The crude product was purified using cyclohexane/ethyl acetate (8.5/1.5, v/v) as the eluent. Yield 49 %. ^{1}H NMR (400 MHz, CD_2Cl_2) δ 10.01 (s, 1H), 7.87 (d, *J* = 8.4 Hz, 2H), 7.74 (d, *J* = 9.1 Hz, 1H), 7.70 (d, *J* = 8.2 Hz, 2H), 7.58 (s, 4H), 7.40 (d, *J* = 16.2 Hz, 1H), 7.32 (d, *J* = 16.2 Hz, 1H), 7.02 (d, *J* = 2.5 Hz, 1H), 6.87 (dd, *J* = 9.1, 2.6 Hz, 1H), 3.44 (q, *J* = 7.0 Hz, 2H), 3.34 (t, *J* = 7.8 Hz, 2H), 1.66 – 1.61 (m, 2H), 1.44 – 1.35 (m, 2H), 1.20 (t, *J* = 7.1 Hz, 3H), 0.98 (t, *J* = 7.4 Hz, 3H).^{13}C NMR (101 MHz, CD_2Cl_2) δ 191.7, 160.9, 147.2, 145.4, 137.6, 137.1, 136.0, 133.9, 132.6, 132.5, 129.9, 129.7, 127.4, 124.4, 123.6, 122.9, 113.1, 102.0, 93.5, 90.32, 51.0, 45.8, 30.0, 20.7, 14.2, 12.5. HRMS (ESI) m/z: [M + H]+ Calcd for $C_{30}H_{29}N_2OS$ 465.2001; Found 465.1999.

Dye **D6.** The crude product was purified using cyclohexane/ethyl acetate (8/2, v/v) as the eluent. Yield 56 %. ^{1}H NMR (400 MHz, CD_2Cl_2) δ 8.02 (dd, *J* = 8.5, 1.8 Hz, 2H), 7.74 (d, *J* = 9.1 Hz, 1H), 7.62 (dd, *J* = 8.5, 1.8 Hz, 2H), 7.58 (s, 4H), 7.40 (d, *J* = 16.2 Hz, 1H), 7.32 (d, *J* = 16.2 Hz, 1H), 7.02 (d, *J* = 2.5 Hz, 1H), 6.87 (dd, *J* = 9.1, 2.6 Hz, 1H), 3.91 (s, 3H), 3.44 (q, *J* = 7.1 Hz, 2H), 3.34 (t, *J* = 7.6 Hz, 2H), 1.66 – 1.59 (m, 2H), 1.44 – 1.35 (m, 2H), 1.20 (t, *J* = 7.0 Hz, 3H), 0.98 (t, *J* = 7.4 Hz, 3H).^{13}C NMR (101 MHz, CD_2Cl_2) δ 166.7, 160.9, 147.2, 145.4, 137.6, 136.9, 133.9, 132.6, 131.9, 130.2, 129.9, 128.1, 127.4, 124.3, 123.6, 123.1, 113.1, 102.0, 92.6, 90.4, 52.5, 51.0, 45.8, 30.0, 20.7, 14.2, 12.5. HRMS (ESI) m/z: [M + H]+ Calcd for $C_{31}H_{31}N_2O_2S$ 495.2106; Found 495.2105.

Cell experiments

Human melanoma A375 cells were obtained from American Type Culture Collection (ATCC, Manassas, VA, USA) and cultured in Dubelcco's Modified Eagle's Medium (DMEM) containing 10% fetal bovine serum (FBS) and 5% penicillin/streptomycin at 37°C in a 5% CO_2 incubator.

Fluorescence imaging

Cultured cells (A375, 5 × 10^4 cells/well) were seeded overnight onto coverslips placed into a 6-well plate and incubated at 37°C in a 5% CO_2 incubator overnight. On the next day, the cover slips were rinsed with PBS, followed by fixation with 4% paraformaldehyde for 5 min, washed with PBS and incubated with the primary antibody for 1 h at RT (EEA1, mouse monoclonal anti-endosome and lamp1, mouse monoclonal anti-lysosome). Next, the coverslips were washed and incubated with the secondary antibody (Alexa Fluor 488 anti-mouse) or Nile Red for 1 h for lipid staining. Finally, the coverslips were washed and mounted on glass slides. Cells were examined using a confocal microscope Nikon A1R scan head on a Nikon Eclipse Ti stand, using a Plan Apo

63× oil 1.4 NA objective. The excitation channel used was a LASER diode 405 nm and the emission signal was collected with an internal PMT detector equipped with a 450/50 filter set, and the transmission signal was collected on an external PMT.

To induce the production of lipid storage vesicles, the cells were treated with oleic acid (100 μM) for 24h before staining with Nile Red or/and **D1**.

Conflict of interest

There are no conflicts of interest to declare.

Acknowledgments

This work was supported by CNRS, University of Nice Sophia Antipolis and University Côte d'Azur, INSERM, Cancéropôle PACA and CAPES (fellowship to MSF, process number 99999.001495/2015-01). We also thank Maéva Gesson for her help with the fluorescence microscopy imaging.

Notes

† These authors (MSF and PD) contributed equally.

Associated Content

Supporting Information: Supplementary figures, copies of ^{1}H, and ^{13}C NMR and HRMS spectra of all reported compounds; spectra from the photophysical study.

References

[1] Thiam AR, Farese R V, Walther TC, Walther TC. The biophysics and cell biology of lipid droplets. Nat Rev Mol Cell Biol 2013;14:775–86. doi:10.1038/nrm3699.

[2] Onal G, Kutlu O, Gozuacik D, Dokmeci Emre S. Lipid Droplets in Health and Disease. Lipids Health Dis 2017;16. doi:10.1186/s12944-017-0521-7.

[3] Danial JSH, Aguib Y, Yacoub MH. Advanced fluorescence microscopy techniques for the life sciences. Glob Cardiol Sci Pract 2016;16. doi:10.21542/gcsp.2016.16.

[4] Zhang X, Wang C, Han Z, Xiao Y. A photostable near-infrared fluorescent tracker with pH-independent specificity to lysosomes for long time and multicolor imaging. ACS Appl Mater Interfaces 2014;6:21669–76. doi:10.1021/am506750m.

[5] Han Y, Li M, Qiu F, Zhang M, Zhang YH. Cell-permeable organic fluorescent probes for live-cell long-term super-resolution imaging reveal lysosome-mitochondrion interactions. Nat Commun 2017;8:1307. doi:10.1038/s41467-017-01503-6.

[6] Zheng X, Zhu W, Ni F, Ai H, Gong S, Zhou X, et al. Simultaneous dual-color tracking lipid droplets and lysosomes dynamics using a fluorescent probe. Chem Sci 2019;10:2342-8. doi:10.1039/C8SC04462G.

[7] Kuimova MK, Yahioglu G, Levitt JA, Suhling K. Molecular Rotor Measures Viscosity of Live Cells via Fluorescence Lifetime Imaging. J Am Chem Soc 2008;50:6672–3. doi:10.1021/ja800570d

[8] Yang Z, He Y, Lee JH, Park N, Suh M, Chae WS, et al. A self-calibrating bipartite viscosity sensor for mitochondria. J Am Chem Soc 2013;135:9181–5. doi:10.1021/ja403851p.

[9] Han J, Burgess K. Fluorescent Indicators for Intracellular pH. Chem Rev 2010;110:2709–28. doi:10.1021/cr900249z.

[10] Yang X, Zhou Y, Zhang X, Yang S, Chen Y, Guo J, et al. A TP-FRET-based two-photon fluorescent probe for ratiometric visualization of endogenous sulfur dioxide derivatives in mitochondria of living cells and tissues. Chem Commun 2016;52:10289–92. doi:10.1039/c6cc05254a.

[11] Roopa, Kumar N, Bhalla V, Kumar M. Development and sensing applications of fluorescent motifs within the mitochondrial environment. Chem Commun 2015;51:15614–28. doi:10.1039/c5cc07098h.

[12] Burke HM, Gunnlaugsson T, Scanlan EM. Recent advances in the development of synthetic chemical probes for glycosidase enzymes. Chem Commun 2015;51:10576–88. doi:10.1039/c5cc02793d.

[13] Huang J, Li N, Wang Q, Gu Y, Wang P. A lysosome-targetable and two-photon fluorescent probe for imaging endogenous β-galactosidase in living ovarian cancer cells. Sensors Actuators, B Chem 2017;246:833–9. doi:10.1016/j.snb.2017.02.158.

[14] Greenspan P, Mayer EP, Fowler SD. Nile red: A selective fluorescent stain for intracellular lipid droplets. J Cell Biol 1985;100:965–73. doi:10.1083/jcb.100.3.965.

[15] Spandl J, White DJ, Peychl J, Thiele C. Live cell multicolor imaging of lipid droplets with a new dye, LD540. Traffic 2009;10:1579–84. doi:10.1111/j.1600-0854.2009.00980.x.

[16] Fam TK, Klymchenko AS, Collot M. Recent advances in fluorescent probes for lipid droplets. Materials 2018;11:1768–87. doi:10.3390/ma11091768.

[17] Niu G, Zhang R, Kwong JPC, Lam JWY, Chen C, Wang J, et al. Specific Two-Photon Imaging of Live Cellular and Deep-Tissue Lipid Droplets by Lipophilic AIEgens at Ultralow Concentration. Chem Mater 2018;30:4778–87. doi:10.1021/acs.chemmater.8b01943.

[18] Jiang M, Gu X, Lam JWY, Zhang Y, Kwok RTK, Wong KS, et al. Two-photon AIE bio-probe with large Stokes shift for specific imaging of lipid droplets. Chem Sci 2017;8:5440–6. doi:10.1039/c7sc01400g.

[19] Wang Z, Gui C, Zhao E, Wang J, Li X, Qin A, et al. Specific Fluorescence Probes for Lipid Droplets Based on Simple AIEgens. ACS Appl Mater Interfaces 2016;8:10193–200. doi:10.1021/acsami.6b01282.

[20] Wang E, Zhao E, Hong Y, Lam JWY, Tang BZ. A highly selective AIE fluorogen for lipid droplet imaging in live cells and green algae. J Mater Chem B 2014;2:2013–9. doi:10.1039/c3tb21675f.

[21] Kang M, Gu X, Kwok RTK, Leung CWT, Lam JWY, Li F, et al. A near-infrared AIEgen for specific imaging of lipid

droplets. Chem Commun 2016;52:5957–60. doi:10.1039/c6cc01797e.

[22] Gao M, Su H, Lin Y, Ling X, Li S, Qin A, et al. Photoactivatable aggregation-induced emission probes for lipid droplets-specific live cell imaging. Chem Sci 2017;8:1763–8. doi:10.1039/c6sc04842k.

[23] Collot M, Fam TK, Ashokkumar P, Faklaris O, Galli T, Danglot L, et al. Ultrabright and Fluorogenic Probes for Multicolor Imaging and Tracking of Lipid Droplets in Cells and Tissues. J Am Chem Soc 2018;140:5401–11. doi:10.1021/jacs.7b12817.

[24] Kim E, Lee S, Park SB. A Seoul-Fluor-based bioprobe for lipid droplets and its application in image-based high throughput screening. Chem Commun 2012;48:2331–3. doi:10.1039/c2cc17496k.

[25] Sharma A, Umar S, Kar P, Singh K, Sachdev M, Goel A. A new type of biocompatible fluorescent probe AFN for fixed and live cell imaging of intracellular lipid droplets. Analyst 2016;141:137–43. doi:10.1039/C5AN01623A.

[26] Goel A, Sharma A, Kathuria M, Bhattacharjee A, Verma A, Mishra PR, et al. New fluoranthene FLUN-550 as a fluorescent probe for selective staining and quantification of intracellular lipid droplets. Org Lett 2014;16:756–9. doi:10.1021/ol403470d.

[27] Appelqvist H, Stranius K, Börjesson K, Nilsson KPR, Dyrager C. Specific Imaging of Intracellular Lipid Droplets Using a Benzothiadiazole Derivative with Solvatochromic Properties. Bioconjug Chem 2017;28:1363–70. doi:10.1021/acs.bioconjchem.7b00048.

[28] Safir Filho M, Fiorucci S, Martin AR, Benhida R. Design, synthesis and photophysical studies of styryl-based push–pull fluorophores with remarkable solvatofluorochromism. New J Chem 2017;41:13760–72. doi:10.1039/C7NJ03142D.

[29] Safir Filho M, Dao P, Gesson M, Martin AR, Benhida R. Development of highly sensitive fluorescent probes for the detection of β-galactosidase activity – application to the real-time monitoring of senescence in live cells. Analyst 2018;143:2680–8. doi:10.1039/C8AN00516H.

[30] Remaining UV-Vis absorption and fluorescence emission spectra are presented in the SI file (Fig. S1).

[31] Baladi T, Granzhan A, Piguel S. Microwave-Assisted C-2 Direct Alkenylation of Imidazo[4,5-b]pyridines: Access to Fluorescent Purine Isosteres with Remarkably Large Stokes Shifts. Eur J Org Chem 2016;2016:2421–34. doi:10.1002/ejoc.201600166.

[32] Mata G, Luedtke NW. Synthesis and solvatochromic fluorescence of biaryl pyrimidine nucleosides. Org Lett 2013;15:2462–5. doi:10.1021/ol400930s.

[33] Estimated using ChemBioDraw 15.0.

[34] Horobin RW, Rashid-Doubell F, Pediani JD, Milligan G. Predicting small molecule fluorescent probe localization in living cells using QSAR modeling. 1. Overview and models for probes of structure, properties and function in single cells. Biotech Histochem 2013;88:440–60. doi:10.3109/10520295.2013.780634.

[35] Rohwedder A, Zhang Q, Rudge SA, Wakelam MJO. Lipid droplet formation in response to oleic acid in Huh-7 cells is mediated by the fatty acid receptor FFAR4. J Cell Sci 2014;127:3104–15. doi:10.1242/jcs.145854.

[36] Würth C, Grabolle M, Pauli J, Spieles M, Resch-genger U. Relative and absolute determination of fluorescence quantum yields of transparent samples. Nat Protoc 2013;8:1535–50. doi:10.1038/nprot.2013.087.

[37] Fulmer GR, Miller AJM, Sherden NH, Gottlieb HE, Nudelman A, Stoltz BM, et al. NMR chemical shifts of trace impurities: Common laboratory solvents, organics, and gases in deuterated solvents relevant to the organometallic chemist. Organometallics 2010;29:2176–9. doi:10.1021/om100106e.